Cortical Actomyosin Flows are Generated by Actomyosin Cluster Vibrations *in Vitro*

Sven K. Vogel[1*], Christian Wölfer[2], Diego A. Ramirez[1,4], Robert J. Flassig[3,5*], Kai Sundmacher[3,6], and Petra Schwille[1*]

[1]Max-Planck Institute of Biochemistry, Am Klopferspitz 18, D-82152 Martinsried, Germany
[2]Process Synthesis and Process Dynamics and [3]Process Systems Engineering, Max Planck Institute for Dynamics of Complex Technical Systems, Sandtorstr. 1, D-39106 Magdeburg, Germany
[4]Graduate School of Quantitative Biosciences, Ludwig-Maximilians-University, Feodor-Lynen-Str. 25, D-81377 Munich, Germany
[5]Brandenburg University of Applied Science, Magdeburger Straße 50, D-14770 Brandenburg, Germany
[6]Department of Process Systems Engineering, Otto von Guericke University Magdeburg, Universitätsplatz 2, D-39106 Magdeburg, Germany

Abstract

Cortical actomyosin dynamics and flows play pivotal roles in eukaryotic cells, e.g. for cell motility, cell division and chiral morphogenesis during early embryogenesis of multicellular organisms. For many model systems myosin motors have been proposed to play a key role in the generation of cortical actomyosin dynamics and flows. However, little is known about the mechanisms behind these actomyosin flows. We reconstituted and confined minimal actin cortices inside water in oil droplets. These spherically confined actomyosin cortices exhibit directional actomyosin flow-like motions upon ATP induced contractility of the myosin motors. By combining our experiments with a theoretical description, we found that the observed direct motion of the actomyosin clusters arises from vibrations within the individual actomyosin clusters. By tracking actin clusters, we detected fingerprints of vibrational states driving their directed motions in the spherical confinement. These vibrations may provide a mechanism driving cortical actomyosin dynamics and flows in living systems.

Introduction

In animal cells cortical actomyosin motions including actomyosin flows have been proposed to drive cell locomotion, cytokinesis, left-right symmetry breaking during embryonic development of multicellular organisms and cellular or tissue chirality (*1-5*). Albeit the omnipresent functions and implications of cortical actomyosin motions and flows, the origin and parameters driving these phenomena are far from being understood. In many eukaryotic model systems myosin motors acting on actin filaments are proposed to play a key role in driving actomyosin dynamics in cytokinetic rings and cortical actomyosin flows (*1, 4, 6-8*). Distinct manipulation of myosin and actin independent other cellular processes is challenging, since they both are functionally highly integrated cellular proteins. Recent studies used the approach of encapsulating frog egg cell extracts in water in oil droplets where manipulation of the protein players may be easier to achieve compared to living systems (*9, 10*). Nevertheless, due to the complex nature of cell extracts similar to living model systems it may be difficult to pinpoint detailed mechanisms and to determine the minimal set of necessary key proteins among the pool of redundant proteins. By a combination of *in vitro* experiments and theory we identified a very likely key mechanism generating actomyosin flow-like motions by myosin motors in a confined spherical environment. We made use of recently developed defined minimal actin cortices (MACs) (*11, 12*) and confined those cortices in water in oil droplets using microfluidics and emulsification techniques. We visualized the formation of a MAC and subsequent actomyosin flow-like motions upon myosin contraction using Spinning Disk microscopy and analyzed their dynamics using Particle Image Velocity methods (*13*).

Results

To encapsulate actin, myosin and anchor proteins inside spherical confinements we made use of microfluidic PDMS based chip technology and droplet formation by emulsification (Fig. 1A). DOPC and biotinylated lipids were dissolved in mineral oil (Supplemental Data). In case of the microfluidic based droplet formation we used a pneumatic microfluidic system where the flow rate of each channel is individually controlled (Fig. 1A, Movie S1). The aqueous solution contained dissolved actin (monomers), neutravidin and myosin in a salt buffer system. In order to test the proper formation of a lipid monolayer that includes biotinylated lipids (DSPE-PEG-2000-Biotin) we started with the encapsulation of fluorescently labeled neutravidin (Oregon Green 488 Neutravidin) (Fig. 1B-D). We show by analyzing the fluorescence intensity through the droplet that neutravidin only binds to the lipid monolayer, when the lipid oil mixture also contains biotinylated lipids (Fig. 1 C and D) indicating that neutravidin does not unspecifically bind to the water/oil interface. Encapsulation of only actin monomers also showed no unspecific binding to the water oil interface (Supplemental Data). Co-encapsulation of myosin motors with the actin monomer and anchor system in the presence of ATP resulted in the formation of a MAC. Inside these droplets actin monomers start to polymerize and bind to the lipid monolayer that contains biotinylated lipids (Figs. 1B and 2A, Movie S2). Concurrently ATP induced contraction of the myosin motors resulted in the formation of actomyosin clusters (Fig. 2B and C, Movie S3). Strikingly, these spherically confined actomyosin clusters undergo directed movement which we will refer to cortical actomyosin motion (CAM) resembling cortical actomyosin flows *in vivo* (Fig. 2A and B; Movies S3 and S5). Note that neither in the absence of ATP nor in the presence of motor inhibitors (Blebbistatin) CAMs were visible (Supplemental Data). We characterized the dynamics of the actomyosin clusters, e.g. the velocity by using particle image velocimetry (*13*) (Fig. 2C; Movie S4). In order to test parameters that change the velocity of CAMs we co-encapsulated a

crowding agent (methycellulose) with various concentrations and found an increase of the velocities in the presence of methylcellulose (Fig. 2D, Compare Movies S3 and S5). By increasing the effective concentration of actin and myosin at the lipid monolayer membrane interface the overall cluster velocity was increased to more than five times. As next step we aimed to determine the mechanism behind myosin driven CAMs and combined our experiments with the formulation of a theoretical description based on biophysical first principle interaction mechanisms, i.e. a priori no explicit movement mechanism have been implemented.

Theory

To understand the migration of individual clusters qualitatively, we modeled the MAC droplet in a continuous, isotropic fluid model. The force generating interaction between actin and myosin is modeled by a simplified myosin cross-bridge cycle (*14-16*) where the force generating confirmation change (r_1) of the myosin head (M) happens immediately after the binding of filamentous F-actin (A) (Fig. 3A). The formed actomyosin complex dissociates after binding of the energy source ATP whose hydrolysis energy reloads the myosin head into the active state (r_2). Usually considered intermediate species have only a very short lifetime (*17*) and are therefore neglected. As the MACs were formed by polymerization, despite the absence of any polymerization or depolymerization regulating proteins in the synthetic *in vitro* system (*18-20*), a rudimentary polymerization cycle (*17*) was added to the model. Thereby, filamentous F-actin depolymerizes (r_3) to monomeric G-Actin with bound ADP (G_D), followed by a spontaneous nucleotide exchange (r_4). ATP bound G-Actin (G_T) binds even stronger to F-Actin (r_5) than G_D (r_6) and thus it is favored over r_6 (*21*). The F-actin filaments, crosslinked by myosin II molecules, forms a mesh-like cortex causing viscoelastic material behavior, which exhibit rheological properties of

a combination of a Maxwell and Kelvin-Voigt model (*22*). The viscoelastic material behavior is considered in the momentum equation (Fig. 3A; Equation [1]) by the passive stress terms, represented by the viscous stress tensor (*23*) and the elastic stress term, with the associated evolution of strain e (Fig. 3A; Equation [2]) (*24*). To describe the active stress, we use a stress term from our previous study (*25*) developed for the present MAC system considering the observed medium ATP-dependency of myosin pulls (*12*). The nondimensionalized species densities are modeled by convection-diffusion equations for convective species (A, A_M, M) and diffusion equation for non-convective species (G_D, G_T, ATP) (Fig. 3A; Equation [3]).

Since the experimental observations show directed movement of individual F-actin clusters, we reduced our analysis to a one-dimensional ring topology. This corresponds to a projection of the spherical droplet and helps to improve the interpretation of the simulation results. Additionally, we assumed that all cortex associated species are located near to the droplet fringe because of fast interactions.

Simulating the PDE system with an inhomogeneous disturbance in myosin initial concentration - which is a reasonable assumption for the *in vitro* system - revealed clustering of a small cluster to a gradually bigger main cluster as it is also observed in the experiments (Fig. 3B and C). Due to the continuous model approach and thus global interconnection of the cluster, the simulated cluster finally merge to one main cluster, in contrast to the observations. Still, one cluster is sufficient to explain the intrinsic motion of an F-actin cluster: The inhomogeneous initial disturbance yields an overall non-symmetric myosin distribution and hence an asymmetric contraction profile as a result of the initial symmetry break.

The final non-symmetric cluster then moves in the one-dimensional ring system like a propagating wave (Fig. 3B and C). Thereby, a non-symmetric contraction profile is preserved by various consumption of the energy source ATP at the leading and trailing edge of the propagating cluster.

Because of the locomotion and the ongoing network depolymerization, the simulated cluster traces non-convective G-actin with bound ADP like a comet tail. In the G-actin tail ATP is additionally consumed for the nucleotide exchange of monomeric actin (r_4) leading to a less steep ATP gradient at the trailing edge of the wave. Thus, less ATP is available for the force generating myosin cross-bridge cycle at the trailing edge of the wave and in the consequence less contractile stress compared to the leading edge (Fig. 3E). Since, the active stress is ATP-driven the wave propagation ceases owing to the ATP depletion (Supplemental Data). In contrast to the experimental setting, we stabilized the ATP concentration (around 0.25), for further investigation of the wave propagation mechanism. Examining the fine structure of the simulated moving cluster reveals an oscillating cluster width with a frequency of approximately 4 periods per time unit for the used parameter set (Supplemental Table1). The fluctuating cluster width is caused by an oscillation of the local ATP concentration and thus oscillation of the passive and active stresses inside of the cluster (Fig. 3D). Thereby, the cluster oscillation passes through the following periodic mechanism.

I. Contraction phase: In the beginning of the contraction phase, a high ATP concentration inside of the cluster results in an increase of the contractile stress and thereby increasing of elastic stress. With progressing contraction, noticeable via a reducing cluster width, the actomyosin species get locally accumulated causing an even stronger contractile stress over the cluster and an increased local ATP consumption.

II. Expansion Phase: When the local ATP concentration falls below a certain threshold, the local energy consumption of the compressed cluster exceeds the available local ATP concentration. In the following, the energy stored in the local network strain widens the cluster. The elastic stress dominates now inside of the cluster. Because of the reduced densities of actomyosin species inside of the cluster and therefore reduced energy consumption ATP fluxes in diffusively and increases the local ATP level.

III. De novo Contraction: Due to the increasing ATP concentration the active contractile stress exceeds the elastic stress. The contractile stress dominates again, and the cluster enters a new contraction phase.

Additionally, an accelerated displacement of center of mass (Fig. 3D) of the cluster, besides the continuous displacement due to inertia, occurs during the contraction phase caused by the unbalanced contraction and therefore higher contraction or deformation at the leading edge. Owing to mass accumulation during the contraction phase the center of mass is not pushed back in the initial position during the expansion phase, despite the unbalanced deformation pattern, which would cause no net movement of the cluster. Hence, oscillating forces due to local ATP depletion and asymmetric cluster contraction are the main drivers of cluster motion. In contrast to previous theoretical studies (*26, 27*), where the necessary asymmetry of self-propagating cluster is caused by polar actin bundles, our suggested model is able to explain also the propagation of cluster of diffusive arranged actin filaments.

For further understanding and as a proof of concept we designed a surrogated rheological model which describes a cluster and exhibits a locomotion caused by the previous described system properties. Thus, we created a three carts spring damper model (Supplemental Data) representing trailing edge, center of mass and the leading edge of the cluster with the viscoelastic material behavior of a Kelvin-Voigt model (*28*). Considering asymmetric oscillating forces, similar contraction and expansion phases are identifiable with viscoelastic forces comparable to the distributed actomyosin model (Supplemental Data).

To find experimental evidence for the theoretically predicted vibrations due to the non-homogeneous distribution of the myosin motors within the clusters we automatically tracked the actomyosin clusters (Fig. 4A). By tracking the directed movement of the individual actomyosin clusters we noticed rotational movements which correlated with a change of the direction of the movement (Fig. 4A and B; Movies S6 and S7). This can be explained by similar vibrations perpendicular to the movement trajectory producing torque, with respect to the center of mass of the cluster. The model predicts vibrations with a certain oscillation period depending on the model time (Fig. 3D). Indications of the existence of vibrations can be found independent of the sampling rate meaning for experimental conditions. For example, a sinusoidal signal having a specific frequency can be measured in undersampling conditions as shown in Figure 4 C. Clearly, the reconstructed signals still conserve the periodic behavior reflected in the Fourier analysis shown in Figure 4D, yet not reflecting the original frequency. Based on this reasoning we analyzed image sequences to measure fluctuations in the distance between geometrical center of mass and intensity-weighted center of mass of several clusters. This clearly represents evidence of the imbalance of mass inside clusters as predicted in the theory. The geometrical center of mass is computed by regular segmentation and binarization which defines the geometry of the cluster whereas the intensity-weighted center of mass is calculated over the same geometry but having the camera-intensity as the statistical weight of every pixel. To be able to combine fluctuations from different clusters, given the different geometry of clusters, we define a characteristic length of the cluster as the square root of the area. As a result, we generate plots of these fluctuations (Fig. 4E). Fourier analysis of theses combined fluctuations strikingly indicates the existence of vibrational states (Fig. 4F, red curve) which are clearly distinguishable from acquisition or camera artifacts (Fig. 4F, grey curve). We interpret the vibrational states as a clear fingerprint of the theoretically predicted vibrations that may provide a mechanism for the directed and rotational movements of the

actomyosin clusters *in silico* and *in vitro*. In conclusion our theory gives evidence that the direct translational and rotational movement of actomyosin clusters originates from an imbalance of oscillatory contractile stresses within the individual actomyosin clusters. Fourier analysis of our experimental data indicates the existence of vibrational states that drive the directional movements of individual actomyosin clusters and the formation of flow-like CAMs in the spherical confinement of the droplets. Hence, for future work it may be of great interest to investigate whether these vibrational states can be found also in cellular model systems that perform myosin driven actomyosin motions, e.g. in cytokinetic actomyosin rings or in cortical actomyosin flows.

Figure 1

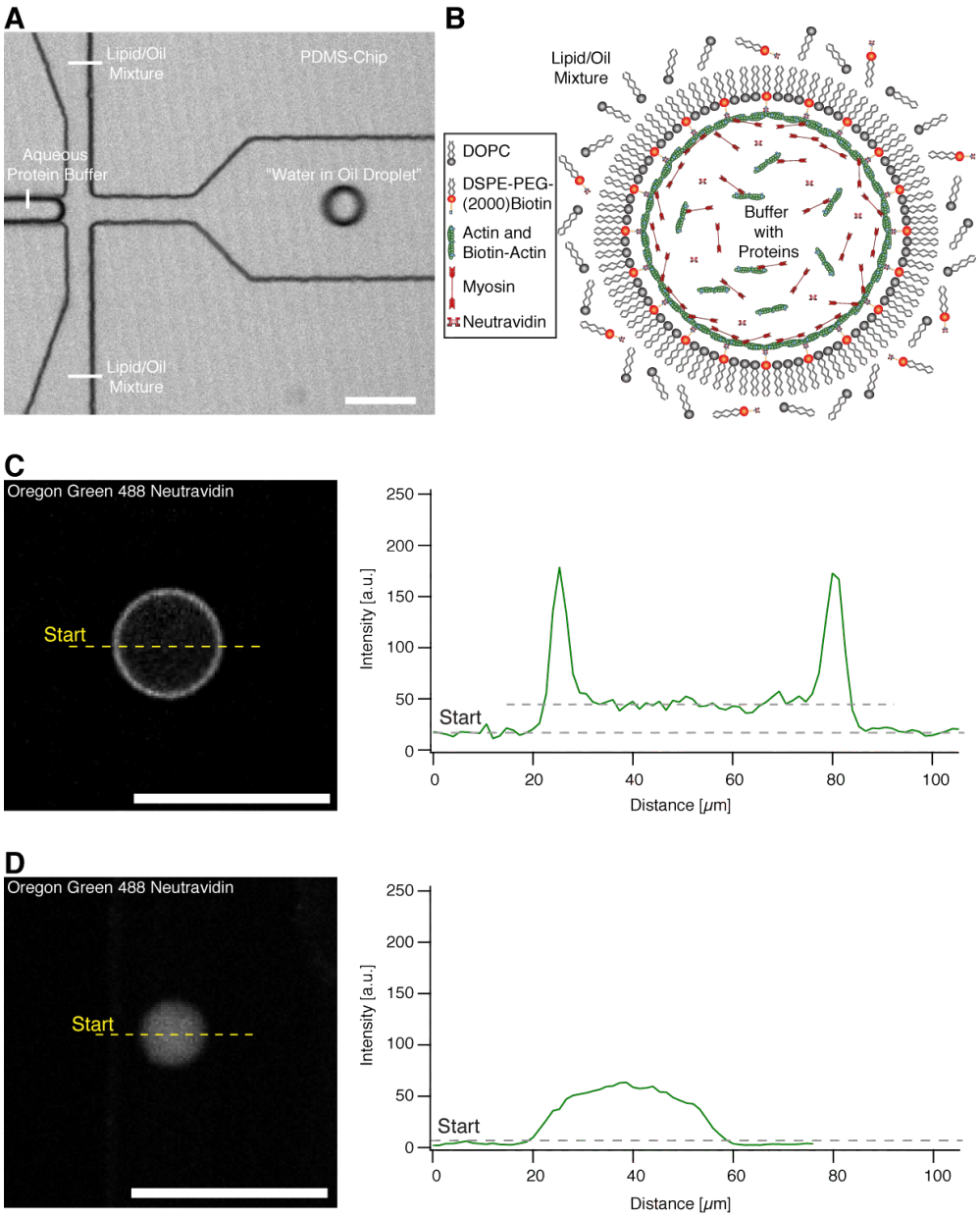

Fig. 1. Encapsulation and actin cortex formation inside water in oil droplets. (A) Confocal Spinning Disk microscope image of a PDMS chip where the encapsulation of the buffer-protein system (see (B)) and formation of the water in oil droplet is shown (Movie S1). (B) Illustration depicting the formation of an actomyosin cortex where actin monomers polymerize to filaments and bind to the lipid monolayer containing biotinylated lipids. The biotinylated actin filaments bind via Neutravidin to the biotinylated lipid anchors. Co-encapsulated myosin motors bind actin filaments and contract the system in an ATP dependent manner. (C) Confocal Spinning Disk microscope image of the equatorial plane of a droplet with a lipid monolayer containing biotinylated lipids showing that encapsulated Oregon green labeled neutravidin binds to the lipid monolayer. Line profile of the fluorescence signal of the Oregon green labeled neutravidin shows two peaks which indicate binding of the neutravidin to the lipid monolayer interface of the droplet (right). (D) In contrast Oregon green labeled neutravidin does not bind to the lipid monolayer and is distributed throughout the lumen of the droplet in the absence of biotinylated lipids. The fluorescence line profile shows no peaks in the absence of biotinylated lipids indicating the absence of unspecific binding to the lipid monolayer (right). Scale bars, 100 μm.

Figure 2

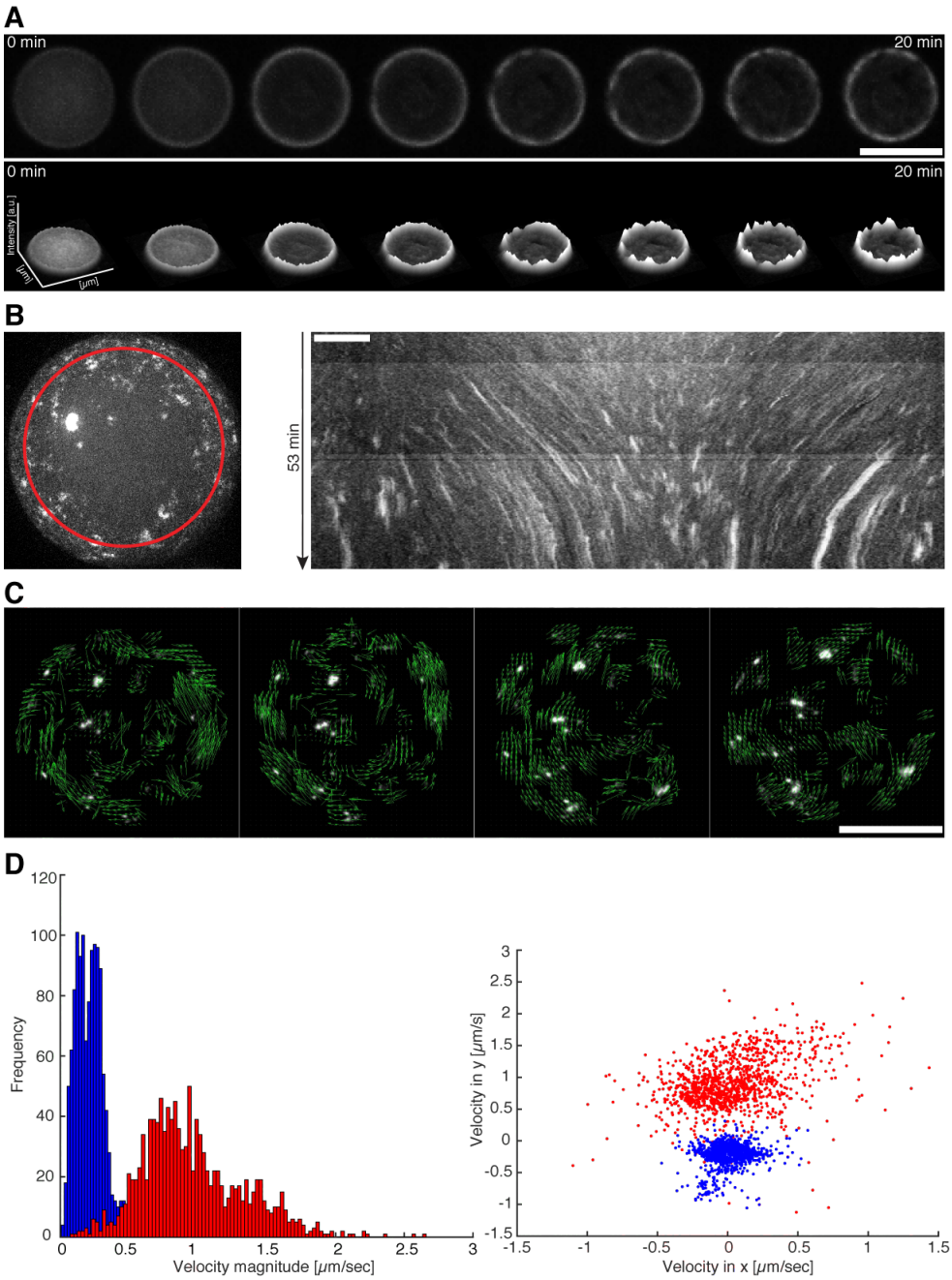

Fig. 2. Directed movement of actomyosin clusters upon ATP dependent actomyosin contraction. (A) Spinning Disk microscope time-lapse images of encapsulated Alexa-488 labeled actin and myosin motors in the presence of ATP at the droplet equator plane. The formation of an actin cortex and actomyosin clusters is shown (upper row) (Movie S2). The respective fluorescent intensity profile indicates the formation of actomyosin clusters and shows their dynamics (lower row). Scale bar 100 µm. (B) Maximum intensity projection of a half droplet confocal Spinning Disk microscope z-stack where Alexa-488 labeled actin clusters are visible (Movie S3). The red circle indicates the path of the generated kymograph (left). A kymograph of the maximum intensity projected half sphere is shown where directed movements of individual clusters represented by distinct lines are visible (right). Scale bar, 10 µm. (C) A Spinning Disk time-lapse image sequence used for particle image velocimetry (PIV) by (*13*). Vectors (green arrows) indicate the flow direction of the directed movement of the actomyosin clusters (Movie S4). Scale bar, 50 µm. (D) Two examples of velocity profiles measured by PIV of droplets with (red) and without a crowding agent (blue) are shown (Movies S3 and S5).

Figure 3

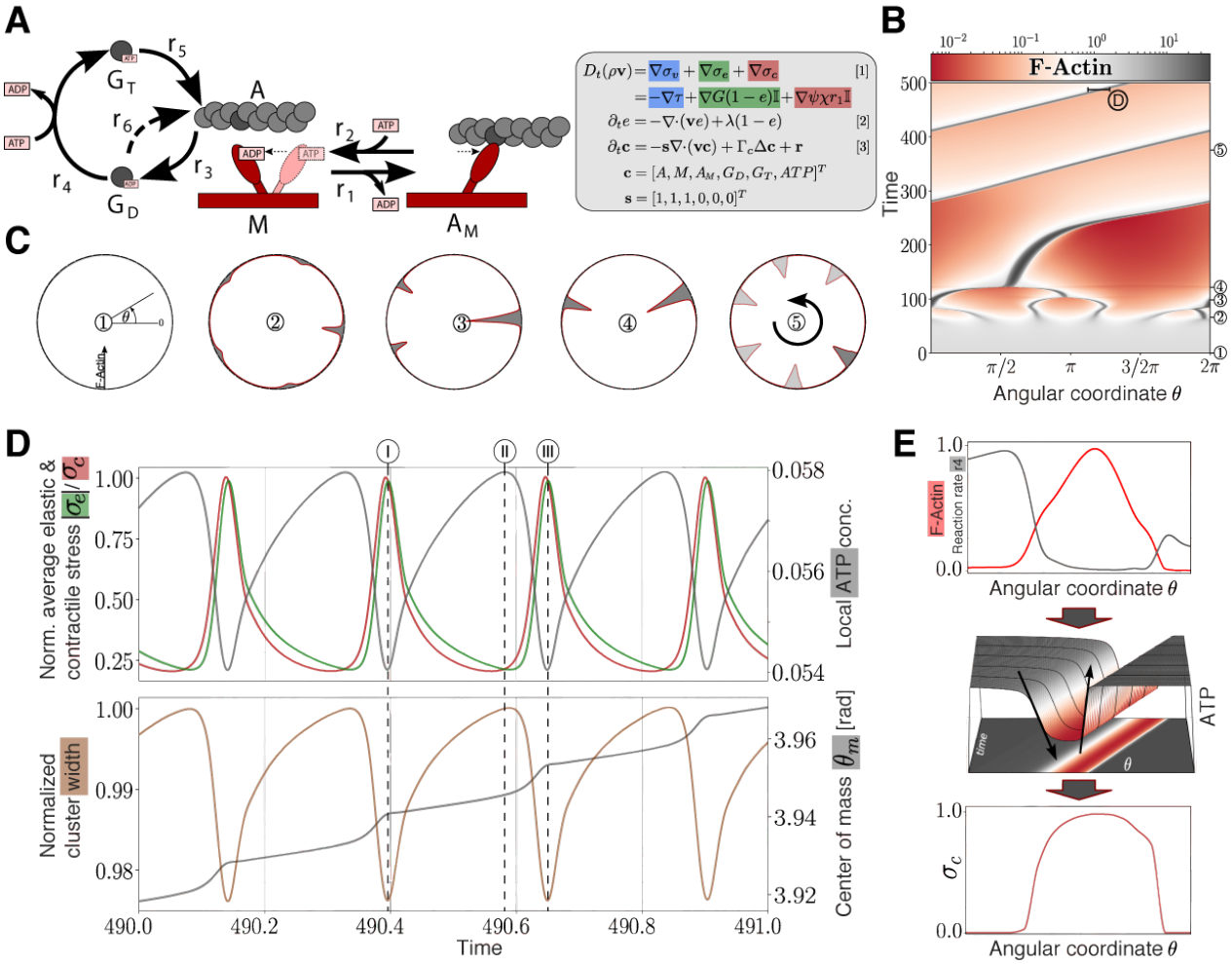

Fig. 3. Modeling and simulation of cortical actomyosin cluster movements reveal vibrations responsible for their movement. (A) Kinetic reaction network with F-actin polymerization cycle and simplified myosin cross-bridge model with corresponding biophysical PDE system. (B) Temporal development of a one-dimensional spatial F-actin distribution with color coded local concentration. (C) Circular representation of distributed F-actin concentration according to the model topology for selected time points (marked in 3B with circles). (D) Vibration of an F-actin cluster. Oscillation over one simulated time unit of average over cluster width of contractile stress σ_c (red) and absolute elastic stress $|\sigma_e|$ (green) normalized by the maximum contractile stress and ATP concentration (gray) in the cluster maximum (upper graph). Additionally, detailed view on evolution of cluster width (brown) normalized by maximum width and displacement of center of mass θ_m (gray) of the F-actin distribution in radiant. Cluster boundaries are defined as the points where the F-actin concentration exceeds the mean concentration (lower graph). (E) Non-symmetric contraction of a propagating cluster. A high activity and therefore high energy consumption of reaction rate 4 (upper graph, gray, normalized) at the trailing edge of the propagating F-actin cluster (upper graph, red, normalized) leads to a sustained non-symmetric ATP distribution (middle graph) around the cluster and, consequently, to an asymmetric contractile stress pattern (lower graph, normalized).

Figure 4

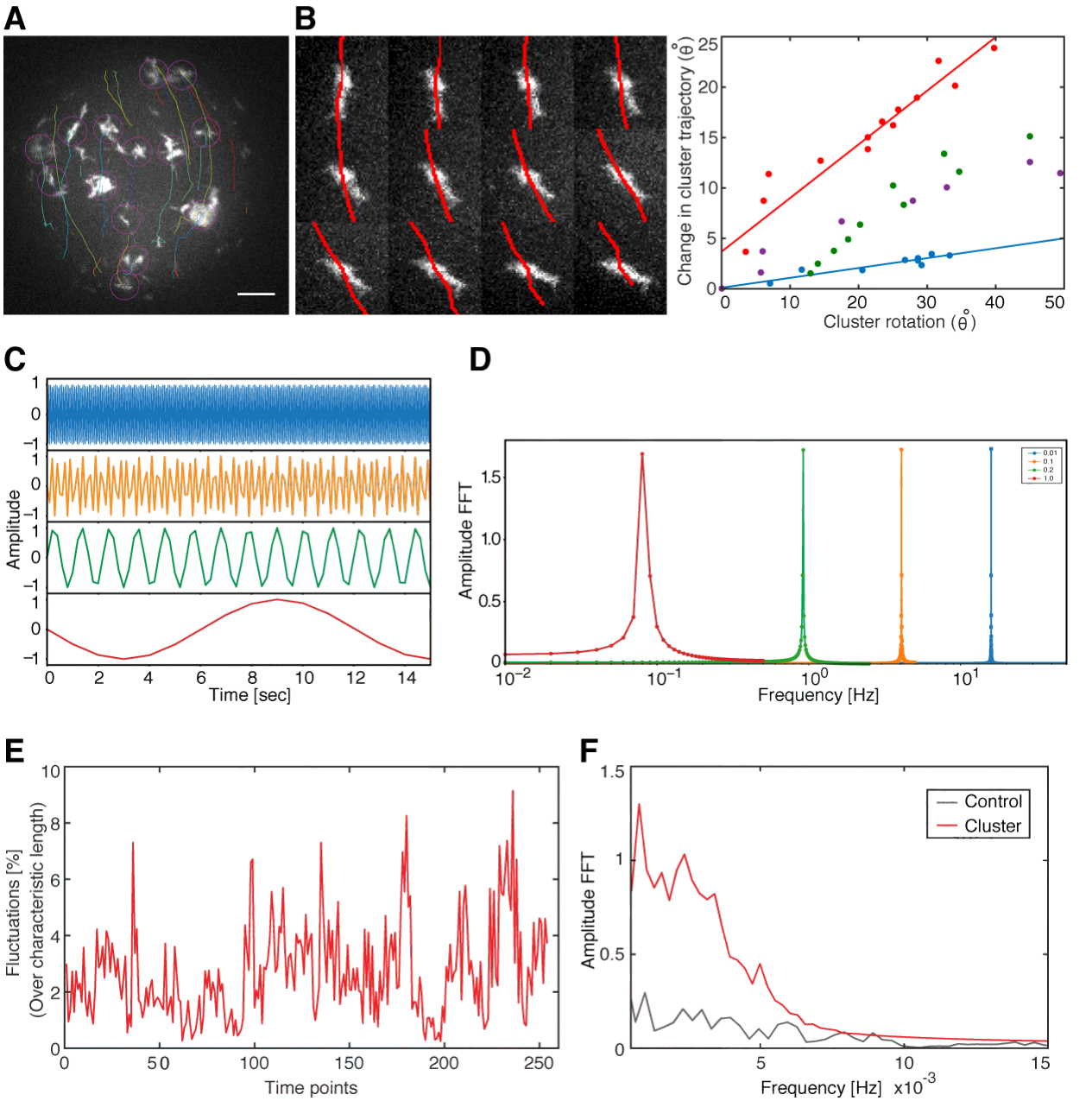

Fig. 4. Fingerprints of actomyosin cluster vibrations during their directed movements. (A) A maximum intensity projection of confocal Spinning Disk microscope images of a half sphere during cortical actomyosin cluster movements is shown. Tracked actin clusters are marked by circles (magenta) and their trajectories shown (various colors, Movie S6). (B) The rotation of clusters along their center of mass agrees with changes in trajectory (red lines) direction (left, Movie S7). Rotation of four independent clusters (various colors) show a correlation (right) between cluster rotation and different rates of steering (different slopes, red and blue line). The red data points correspond to the montage shown on the left. (C) A simulated sinusoidal signal with an angular frequency of 100 ms that has been sampled every (D) 10 ms (blue), 100 ms (orange), 200 ms (green) and 1 sec (red). As a proof of principle, independent of the sampling rate, Fourier analysis enables to establish a fingerprint of the original signal frequency. (E) Time traces displaying more than 20 combined cluster vibrations (red). The amplitude of the vibrations is normalized with respect to the characteristic length of the cluster (here defined as the square root of the cluster). Therefore, respective vibrations from individual clusters are concatenated to have a representative time signal. (F) The fast Fourier transformation (FFT) indicates the presence of vibrational states (red) different from acquisition artifacts (grey). Scale bar, 10 µm.

Acknowledgements

We are grateful for the financial support by the Daimler und Benz foundation (Project Grant PSBioc8216), the Gottfried Wilhelm Leibniz-Program of the DFG **(**SCHW716/8-1**),** the support of the Graduate School of Quantitative Biosciences Munich and the MaxSynBio consortium, which is jointly funded by the Federal Ministry of Education and Research of Germany and the Max Planck Society.

References

1. D. Bray, J. G. White, Cortical flow in animal cells. *Science* **239**, 883-888 (1988).
2. R. N. Khaliullin *et al.*, A positive-feedback-based mechanism for constriction rate acceleration during cytokinesis in Caenorhabditis elegans. *Elife* **7**, (2018).
3. S. R. Naganathan, T. C. Middelkoop, S. Furthauer, S. W. Grill, Actomyosin-driven left-right asymmetry: from molecular torques to chiral self organization. *Curr Opin Cell Biol* **38**, 24-30 (2016).
4. V. Wollrab, R. Thiagarajan, A. Wald, K. Kruse, D. Riveline, Still and rotating myosin clusters determine cytokinetic ring constriction. *Nature communications* **7**, 11860 (2016).
5. A. C. Callan-Jones, R. Voituriez, Actin flows in cell migration: from locomotion and polarity to trajectories. *Curr Opin Cell Biol* **38**, 12-17 (2016).
6. E. Munro, J. Nance, J. R. Priess, Cortical flows powered by asymmetrical contraction transport PAR proteins to establish and maintain anterior-posterior polarity in the early C. elegans embryo. *Developmental cell* **7**, 413-424 (2004).
7. S. R. Naganathan, S. Furthauer, M. Nishikawa, F. Julicher, S. W. Grill, Active torque generation by the actomyosin cell cortex drives left-right symmetry breaking. *Elife* **3**, e04165 (2014).
8. M. Nishikawa, S. R. Naganathan, F. Julicher, S. W. Grill, Controlling contractile instabilities in the actomyosin cortex. *Elife* **6**, (2017).
9. K. Suzuki, M. Miyazaki, J. Takagi, T. Itabashi, S. Ishiwata, Spatial confinement of active microtubule networks induces large-scale rotational cytoplasmic flow. *Proc Natl Acad Sci U S A* **114**, 2922-2927 (2017).
10. T. H. Tan *et al.*, Self-organized stress patterns drive state transitions in actin cortices. *Sci Adv* **4**, eaar2847 (2018).
11. S. K. Vogel, F. Heinemann, G. Chwastek, P. Schwille, The design of MACs (minimal actin cortices). *Cytoskeleton (Hoboken)* **70**, 706-717 (2013).
12. S. K. Vogel, Z. Petrasek, F. Heinemann, P. Schwille, Myosin Motors Fragment and Compact Membrane-Bound Actin Filaments. *eLife* **2013;2:e00116**, (2013).
13. W. Thielicke, PIVlab – Towards User-friendly, Affordable and Accurate Digital Particle Image Velocimetry in MATLAB. *Journal of Open Research Software* **2(1):e30**, (2014).
14. H. E. Huxley, The mechanism of muscular contraction. *Science* **164**, 1356-1365 (1969).
15. R. W. Lymn, E. W. Taylor, Mechanism of adenosine triphosphate hydrolysis by actomyosin. *Biochemistry* **10**, 4617-4624 (1971).

16. J. A. Spudich, The myosin swinging cross-bridge model. *Nat Rev Mol Cell Biol* **2**, 387-392 (2001).
17. J. Howard, in *Mechanics of motor proteins and the cytoskeleton,* J. Howard, Ed. (Sinauer Associates Inc. {a} , 23 Plumtree Road, Sunderland, MA, 01375, USA, 2001).
18. T. D. Pollard, G. G. Borisy, Cellular motility driven by assembly and disassembly of actin filaments. *Cell* **112**, 453-465 (2003).
19. T. D. Pollard, J. A. Cooper, Actin, a central player in cell shape and movement. *Science* **326**, 1208-1212 (2009).
20. L. Blanchoin, R. Boujemaa-Paterski, C. Sykes, J. Plastino, Actin dynamics, architecture, and mechanics in cell motility. *Physiol Rev* **94**, 235-263 (2014).
21. T. D. Pollard, I. Goldberg, W. H. Schwarz, Nucleotide exchange, structure, and mechanical properties of filaments assembled from ATP-actin and ADP-actin. *The Journal of biological chemistry* **267**, 20339-20345 (1992).
22. A. Mogilner, Mathematics of cell motility: have we got its number? *J Math Biol* **58**, 105-134 (2009).
23. R. B. Bird, W. E. Stewart, E. N. Lightfoot, *Transport phenomena*. (John Wiley and Sons, Inc., New York, 1960, 1960).
24. O. L. Lewis, R. D. Guy, J. F. Allard, Actin-myosin spatial patterns from a simplified isotropic viscoelastic model. *Biophys J* **107**, 863-870 (2014).
25. C. Wölfer, S. K. Vogel, M. Mangold, A curvilinear Model Approach: Actin Cortex Clustering Due to ATP-induced Myosin Pulls. *Ifac Papersonline* **49**, 103-108 (2016).
26. K. Kruse, S. Camalet, F. Julicher, Self-propagating patterns in active filament bundles. *Phys Rev Lett* **87**, 138101 (2001).
27. F. H. Kreten, C. Hoffmann, D. Riveline, K. Kruse, Active bundles of polar and bipolar filaments. *Phys Rev E* **98**, (2018).
28. W. Voigt, Ueber innere Reibung fester Körper, insbesondere der Metalle. *Annalen der Physik und Chemie* **283**, 671-693 (1892).